

Comparison of five strategies for seasonal prediction of bioclimatic indicators in the olive sector



Chihchung Chou^{a,d,*}, Raül Marcos-Matamoros^{a,b}, Javier López-Nevado^c, Silvia López-Feria^c, Nube González-Reviriego^a

^a Earth Sciences Department, Barcelona Supercomputing Center – CNS, Plaça d'Eusebi Güell, 1-3, Barcelona 08034, Spain

^b Department of Applied Physics, University of Barcelona, Av. Diagonal 647, Barcelona 08028, Spain

^c Research, Development and Innovation Department, Dcoop Sociedad Cooperativa Andaluza, Ctra. de Córdoba S/N -Apdo 300-, 29200 Antequera (Málaga), Spain

^d now at: Climate Change Division, the National Science and Technology Center for Disaster Reduction, No. 200, Sec. 3, Beixin Rd., Xindian District, New Taipei City, Taiwan

ARTICLE INFO

Keywords:
Climate services
Seasonal prediction
Olive sector
Bioclimatic indicator
Blending strategy

ABSTRACT

This paper assesses the forecast quality of five seasonal forecasting strategies applied to different bioclimatic indicators tailored to the olive sector. In total, five indicators have been selected considering their importance in the management of the olive orchard. As time progresses through the indicator target period, the impact of the increasing share of actual observations included in its computation has been evaluated by examining the variabilities of correlation coefficients and fair rank probability skill scores for each initialization date. The results show that blending either seasonal predictions or climatology with observations enhanced the capability of forecasting the tercile category for all the indicators when compared to the use of climatology or seasonal predictions alone. In fact, for Spring Maximum Temperature and Growing Season Temperature indicators, the combination of observations and SEAS5 predictions could outperform the other methods for most of the start months. As for those threshold-defined indicators, namely Spring Heat Days and Summer Heat Stress Days, the end-users are highly encouraged to use climatology in the first month and combine it with observations as soon as the latter becomes available.

Practical implication

Olives, one of the essential staples in many Mediterranean countries, have contributed to society both culturally and ecologically for millennia (Besnard et al., 2013). For instance, the Mediterranean and Southern Spain accounted for more than half of the total areas of olive trees (i.e., five million hectares) in the European Union (Rossi et al., 2017) in 2020–2021. However, this area faces critical challenges, with climate change projections showing a significantly hotter and drier climate towards the end of this century (Carvalho et al., 2021; Cook et al., 2020; Giorgi and Lionello, 2008; Lee et al., 2021; Cos et al. 2022). Given these complex scenarios, the scientific community has suggested that user-driven climate services could be an increasingly valuable tool to tackle these foreseen risks and impacts (Ranasinghe et al., 2021).

In this framework, seasonal predictions have already been applied to various agricultural sectors with varying degrees of success (Ceglar and Toreti, 2021; Izumi et al., 2021). More specifically, the combination of observations and seasonal predictions within the calculation of bioclimatic indicators (hereafter blending strategy) could enhance the forecast skill of seasonal predictions when applying this strategy to the wine sector. Therefore, this work aims to study the potential of improving seasonal forecasts in the Iberian Peninsula (IP) by using five methods (including the blending mentioned above) to five bioclimatic indicators for the olive sector.

The results support the future uptake of observations when predicting sectoral indicators because there would be higher correlations and fair Rank Probability Skill Score (fair RPSS) in the earlier months of the indicator target period. In fact, the end-users are encouraged to combine observations and SEAS5 prediction for the Spring Maximum Temperature (SPRTX) and Growing Season Temperature (GST) indicators over the IP. Regarding the

* Corresponding author.

E-mail address: chihchung.chou@bsc.es (C. Chou).

threshold-defined indicators such as Spring Heat Days (SPR32) and Summer Heat Stress Days (SU36 and SU40), the observed climatology is preferable in the first month and combined with observations as soon as the latter becomes available.

To conclude with the practical implication, this work could be a general guideline for the olive sector end-users when they prepare the bioclimatic indicators based on seasonal predictions by making the most of all the accessible information.

Data availability

Data will be made available on request.

Introduction

Cultivation of olive trees has been established in the Mediterranean region for centuries (Besnard et al., 2018). In addition to being an essential staple, the olive became essentially representative in the cultural, ecological and economic aspects after its domestication (Besnard et al., 2013). In 2020–2021, the European Union (EU) accounted for 68 % and 32 % of the world's olive oil and table olives production, respectively (IOC, 2018). Furthermore, the EU's approximately-five million hectares of olive trees return 7.000 million euros yearly (Rossi et al., 2017). Across the southern European countries, Mediterranean Spain is one of the main pillars in the olive industry, holding more than half of the total cultivation areas, followed by Portugal, Greece, France, Croatia, Italy, etc.

Like other crops, olive trees are sensitive to changes in the climate. For instance, in general, olive production was found to be negatively correlated with maximum and minimum temperature, particularly in spring and summer. Additionally, the severely arid condition due to the increases in evapotranspiration during extremely hot days, was also shown to negatively affect the olive tree growth (Zimmermann et al., 2015; Orlandi et al., 2020). Actually, the long-term CMIP5 and CMIP6 projections for this region agree that this climatic situation is likely to continue or even worsen in the foreseeable future (Guioit and Cramer, 2016; Cos et al., 2022). Consequently, the uncertainties linked to this climate evolution can lead to unavoidable risks for the sector.

The global and regional climate models under varying IPCC pathways projected a significantly hotter and drier Mediterranean basin by the end of the 21st century (Carvalho et al., 2021; Cook et al., 2020; Giorgi and Lionello, 2008; Cos et al., 2022). Specifically, up to 6.5 °C of summer warming could be observed in the Mediterranean region in 2070–2099 than in 1971–2000 (Kröner et al., 2017; Brogli et al., 2019). A more considerable variability would happen due to one season with more hot days. Moreover, the projection of heat waves from regional climate models was increased from ten days/year to above 50 in the Mediterranean by the end of this century (Molina et al., 2020; Kuglitsch et al., 2010). Furthermore, a drier southern Mediterranean was projected in terms of the annual total precipitation by 2050, while up to 25 % of the increase in the 50-year precipitation extreme was simultaneously seen (Zittis et al., 2021). The above challenges warn that an advanced strategy of adaptation and preparedness is urgently required and needs to be tailored to the olive sector by using reliable climate information (Ranasinghe et al., 2021).

Seasonal predictions have served as a readily useful tool of adaptation in the field of agriculture (Vajda and Hyvärinen, 2020), namely wine grape, wheat (Ceglar and Toreti, 2021), and other crops (Hayashi et al., 2018). Through co-developing with the end-users, the seasonal forecasts of the Essential Climate Variable (ECV) and the bioclimatic indicators tailored to the sector of interest provide promising values in their process of decision-making (Giannakopoulos et al., 2020; Marcos-Matamoros et al., 2020). For example, the olive-sector agronomists argued that the weather information from the forthcoming week to

months is the most useful when making key decisions (Sanderson et al., 2019). Specifically, fertilization occurs from March to October; irrigation is applied from April to October, and soil labor must be well arranged throughout the year (Sanderson et al., 2019). As such, key proxies which were identified by the olive company DCOOP (in the MED-GOLD project) could enlighten the aforementioned critical decisions (Giannakopoulos et al., 2019).

Following the finding of the increase in the forecast skill when applying the blending strategy to the wine sector, five bioclimatic indicators of the olive sector were used to assess its transferability by comparing the performance of the predictions from five blending strategies. The structure of this paper is as follows. In the next section, the data sets and the spatial domain are first introduced. After that, in section 3, the definitions of the selected bioclimatic indicators, the five blending strategies, and the methods for the subsequent evaluation are presented. Next, section 4 exhibits the quality comparison of the forecasting strategies for each indicator and initialization date (i.e., each month of the indicator period). Finally, conclusions and suggestions are summarised in section 5.

Data and spatial domain

The lead time zero predictions of daily temperature data (including maximum, mean and minimum) from the European Center for Medium-Range Weather Forecasts (ECMWF) SEAS5 (denoted as S5 hereafter, Johnson et al., 2019) were used in this work (downloaded from the C3S-CDS, Raoult et al., 2017). The Integrated Forecast System (IFS) Cycle 43r1 was used in the S5 prediction model (Copernicus version). The aforementioned ECVs were provided as forecasts of seven months into the future with 25 ensemble members at one-degree spatial resolution (Johnson et al., 2019; Gubler et al., 2019; Weisheimer et al., 2020). The reference data, used for the blending, bias correction and verification was the ECMWF ERA5 reanalysis (Hersbach et al., 2018). As for the reference data, we used the ECMWF ERA5 reanalysis with a resolution of 0.25° (Hersbach et al., 2018; Hersbach et al., 2020). The ECVs used were the same 3 types of temperature (minimum, maximum and mean) covering the 1993–2016 period.

Regarding the spatial domain, the IP remains the key region because more than half of the five million hectares where the olive trees are cultivated in the EU are located in its southern part as shown in Fig. 1. The geographical location of the IP, in between the North Atlantic Ocean and the Mediterranean Sea, determines its unique climatic condition for the olive groves.

Methodology

Bioclimatic indicators

Dcoop is one of the leading world producers of olive oil, contributing with an average 8 % to the total global production (~0.23 million tonnes out of 3 million grand total, according to 2021 data). During the co-development process with this end-user, temperature showed to be of particular interest because it affects the phenological cycle of olive trees from winter to autumn and establishes the magnitude of pests' impacts as well as water requirements. Consequently, five temperature-based bioclimatic indicators were selected due to their importance and usefulness from the olive sector perspective (see Table 1). Additionally, Table s1 outlines the functions in the CSIndicators R-package (Pérez-Zanón et al., 2021) that were used for the calculation of the indicators in this paper.

The first indicator, Spring Maximum Temperature (SPRTX), is the mean maximum temperature from April-May. The mean condition of springtime's highest temperature is important for hydrologic stress (e.g., evapotranspiration), flowering, pollination, and pest treatment (Sanderson et al., 2019). For example, the olive moths (*Prays oleae*) could appear when the temperature in spring is mild and attack the different

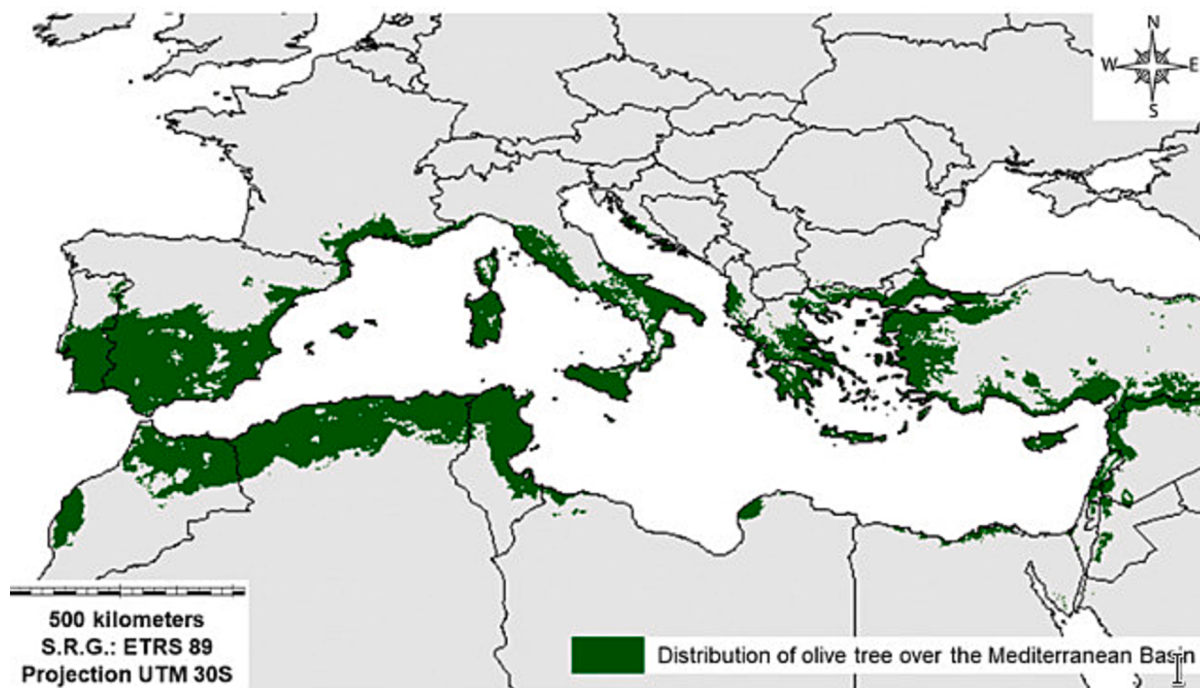


Fig. 1. Distribution of olive trees in the Mediterranean Basin (Rodríguez Sousa et al., 2020).

Table 1

Description of the associated impacts, relevant decisions and potential value of the seasonal predictions for the bioclimatic indicators analysed in this paper.

Indicator	Period	Associated impact	Relevant decision	Potential value
Spring Maximum Temperature	April and May	Flowering, flower-to-fruit conversion, olive moth attack rate and pollination efficiency	Phytosanitary treatment, fertilization and production forecast.	End-users could increase the responsible use of phytosanitary products, optimize fertilizer application and, based on production forecasts, make better market decisions.
Spring Heat Days	From 21st April to 21st June	Onset of flowering, pollination efficiency and fruit setting.	Irrigation planning and production forecast.	End-users could optimize the use of water and, based on better crop prediction, make better market decisions.
Summer Heat Stress Days	From 21st June to 21st September	Olive fly attack rate and water deficits	Protection of plants and need for irrigation	End-users could increase the responsible use of phytosanitary products and optimize the use of water
Growing Season Temperature	From April to October	Water/nutrient deficit level	Irrigation, fertilization and production forecast.	End-users could optimize the use of water and fertilizer products and, based on production forecasts, make better market decisions.

parts of the olive: leaves, flowers, and newly set fruit through some of its three annual generations. Therefore, this indicator can inform the potential locations before its emergence. Moreover, reactions to control the pest, such as the use of phytosanitary treatments, can be improved in advance (MED-GOLD, 2021).

Another springtime indicator is Spring Heat Days (SPR32). The definition is the accumulated number of days with the maximum temperature exceeding 32 °C from 21st April to 21st June. SPR32 is relevant to various decision-making, from plant treatment before flowering (Ozdemir, 2016) and irrigation planning to the prediction of crop production. For example, flowering may occur earlier if a higher temperature (above 30 °C) is seen in early spring. As such, the subsequent pollination will happen earlier, too (Sanderson et al., 2019).

The other two indicators for summertime are Summer Heat Stress Days (i.e., SU36 and SU40), which represent the accumulated days with the daily maximum temperature above 36 and 40 °C, respectively, from 21st June to 21st September. Since there are more olive fruit flies in this season, both indicators can not only inform the protection of plants (e.g., avoid lowering the quality due to the olive fly pest) but also hint at the need for irrigation (e.g., against heat stress or drought, Tognetti et al., 2004). Advanced reactions are critical from May onwards, throughout the summer, and sometimes until October (MED-GOLD, 2021). Besides, the variability of olive pollen was significantly reduced for 11 cultivars (out of 12) when the temperature of 36 °C was maintained in an

experiment conducted at a relatively high level of wetness (Iovane et al., 2021). As such, 36 and 40 °C could represent extreme weather conditions for the locations where pollination occurs in summer.

Lastly, the Growing Season Temperature (GST) indicator is the 7-month average of daily mean temperatures from April to October. This indicator is critical because both temperature maximum and minimum are taken into account, and the operations such as irrigation and fertilization are mainly conducted during this period. Besides, this 7-month period is associated with the two phases with a higher vegetative growth rate (above 50 %) of the biannual pattern of olive trees (Benlloch-González et al., 2019). As such, GST is paramount not only due to its phenological meaning but also because its longer time slot helps better understand the variability of performances with the increasing proportion of observations in the indicator.

Five blending strategies for predicting the indicators

This section describes the five strategies to predict the bioclimatic indicators seasonally. Their descriptions and acronyms are tabulated in Table 2. The first two predictions were ERA5 climatology (E5) and bias-corrected SEAS5 predictions (S5). In addition, the B-S5 and B-E5 (standing for Blending-SEAS5 and Blending-ERA5) progressively combined the past observations (when available) with, respectively, the SEAS5 predictions and the ERA5 climatology. Fig. 2 depicts the data sets used in each indicator target month (SPRTX) for both B-S5 and B-E5. The

Table 2

Description of the Predictions from the Five Strategies.

Acronyms	Construction of Data	Remarks
E5	ERA5 climatology	E5 was used as a benchmark in this work (when computing the FRPSS).
S5	Bias corrected SEAS5 predictions (the first start month only)	The variance inflation method (Von Storch and Zwiers, 2002), assessed in Doblas-Reyes et al. (2005) , was applied for the bias adjustment in this work.
B-S5	SEAS5 predictions blended with the past observations	See Section 3.2.1 for more details and Fig. 2 for a schematic plot
B-E5	Ensemble ERA5 climatology blended with the past observations	
P	Persistent prediction	See Section 3.2.2 for details

detailed steps for generating B-S5 and B-E5 were explained in Section 3.2.1. Last but not least, the persistence method (P) was the fifth approach included in the comparison (see section 3.2.2 for more details).

The B-S5 and B-E5 strategy

The construction of B-S5 and B-E5 approaches follow a blending strategy. In this procedure, as the time moves forward through the indicator-defined period (e.g. GDD, advancing from April to October), the most recent prediction ‘blends’ with the observations that have progressively become available. Consequently, as time comes by, the prediction of the indicator is a combination of observed and forecast information. That said, the forecast portions of B-S5 and B-E5 are different. In B-E5, the forecast is an ensemble based on the resampling of past ERA5 climatology (25 members obtained with bootstrap and cross-validation methods), whereas the B-S5 forecast is the 25-member ensemble from SEAS5 hindcast. To better visualise these differences, [Fig. 2](#) shows a schematic diagram for both B-S5 and B-E5 based on a SPRTX use-case.

1. Load ERA5 daily temperature maximum for April and May over IP from 1993 to 2016
2. To generate the ensemble observations for B-E5, resample the above daily ECV with bootstrap and cross-validation methods (25 ensemble members). For instance, for the year 1993, one out of the 23 years (from 1994 to 2016, excluding the current year) was randomly selected 25 times with replacements (i.e., one year could be used

twice or more). After that, there would be 25 members for the year 1993. This resampling was repeated throughout the entire period to obtain a full observational ensemble (see the green cells in ‘Apr’ columns of B-E5 in [Fig. 2](#)). This ensemble observation was then considered as the ‘predictions’ such as SEAS5 predictions in B-S5 and was then combined with the past observations described in step 3.

3. When the season proceeded, the above B-E5 and B-S5 were combined with the past observations: April observations became available in May, so the original April data (i.e., the blue and green cells in ‘Apr’ columns of B-S5 and B-E5 in [Fig. 2](#)) were substituted with the past data (i.e., the yellow cells in ‘May’ columns) for all the members. After the replacements, the SPRTX indicators for the start month of May were computed for B-S5 and B-E5.

The B-E5 predictions, particularly for those indicators associated with a specific threshold, might not share a similar statistical distribution as observed in the ERA5 because of the likely inherent bias seen in dynamic prediction models. Therefore, for the threshold-defined indicators (including SPR32, SU36 and SU40), the percentile corresponding to the absolute threshold used in the observation was translated to a new threshold (see the formula in [Table s1](#)) before computing the indicators. This adjusted threshold not only holds the same position as the original threshold in the observed data but also avoids the non-surpassing scenario (i.e., the latter was too extreme for some seasons/locations). Thus, this adjustment implicitly contains a bias correction ([Casanueva et al., 2018](#)). It is worth mentioning that the S5 and B-S5 predictions of the indicators were bias-corrected with the calibration method ([Von Storch and Zwiers, 2002; Doblas-Reyes et al., 2005](#)) before computing the skill metrics by using ERA5 as the reference dataset. Taking into account the adjusted threshold and the combination with observations (blending approach), only one bias-adjustment method was applied in this work. Hence, in the near future it may be worth investigating other bias correction methods (e.g., quantile mapping and others being compared in [Manzanas et al., 2019](#)). Besides, the climate change signal has not been explicitly considered in this study so it can also be a topic for future research.

The persistence strategy

The assumption of the persistence method is that tomorrow remains the same as today. As such, this approach is expected to work well when the climate is relatively stable within the timescale of interest. In this work, two types of persistence methods were applied according to the characteristics of the indicators: an adjusted one for the threshold-

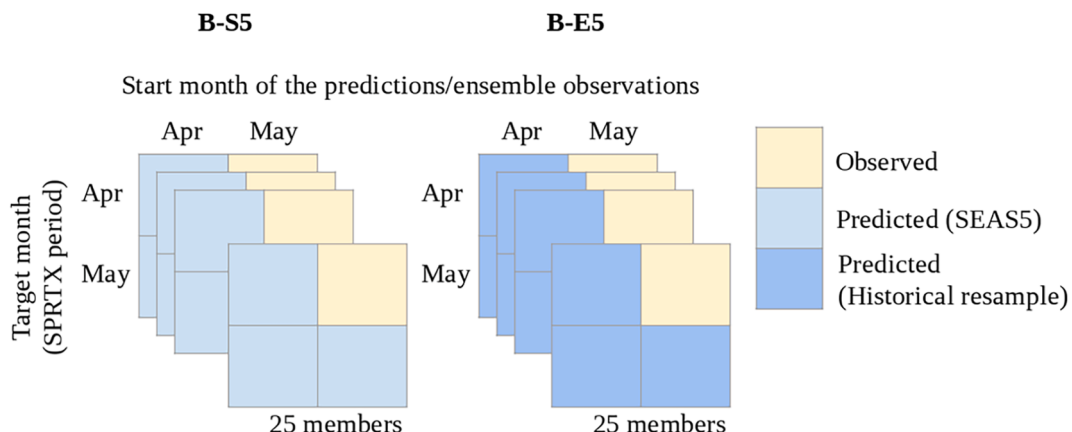


Fig. 2. Schematic diagram for the B-S5 and B-E5 blending strategies (taking SPRTX as an example). The yellow, blue and dark blue cells represent, respectively, the past observations, SEAS5 predictions and the resampled observations (climatology). There are 25 ensemble members for each of the start months (April and May, column-wise) and both B-S5 and B-E5. For the start month of April (the ‘Apr’ columns), the ensemble SEAS5 predictions (the blue cells) and the ensemble observations (the dark blue cells) were used to compute SPRTX for B-S5 and B-E5 without replacements, respectively. When the season progressed to May, the April observations became available. The ‘Apr’ cells in the ‘May’ columns were thus replaced with the past observations (i.e., the yellow cells for both cases). (For interpretation of the references to color in this figure legend, the reader is referred to the web version of this article.)

defined indicators and the original one for the period-average ones.

1. 1 Original persistence method

Complying with the aforementioned concept, the key step is to decide the month(s) used for each initialization date. To uptake as much information from observations as possible, we tried to use all the days of the closest month(s) being available. Taking GST as an example, the daily data in March (April) was taken to compute the indicator for the start month April (May). Thereafter, from the start month June onwards, the months from April to the month before the present were used. For instance, the start month July took the daily data from April to June and the final start month took the past six months. The temperature averaged over the selected month(s) represented the prediction of the indicator for that initialization date.

2. Adjusted persistence method

Since the fixed temperature threshold might not be fair to be used in all the months of the defined period for determining the exceedance, the percentile corresponding to the threshold taking into account the entire period was calculated and used. In other words, a new temperature threshold that corresponds to the same percentile would be translated by taking the selected months for each start month. Taking SPR32 as an example, we first computed the percentile corresponding to 32 °C considering all the days from 21 April – 21 June. Secondly, for the start month April (May), a new threshold matching the percentile could be calculated by taking into account the daily data in March (April). After that, the indicator would be the accumulated number of days when the daily temperature maximum exceeded the revised threshold in March (April). The above adjustment avoids generating many zeros because the original threshold could be difficult to reach in a cooler month. Besides, the modified threshold reasonably represents a crossing point for the month(s) selected in each initialization date.

Evaluation methods

To evaluate the predictions obtained from the five strategies, both deterministic (including bias and correlation coefficient) and probabilistic (i.e., fair RPSS, Fricker et al. 2013; Ferro 2014) metrics were used. Further, these verification metrics were computed for each initialization date of the indicator target period to understand the effect of the increasing share of the observations within the indicator on the forecast quality.

The fair RPSS was calculated with the leave-one-out strategy and the interannual average was presented in the results. Moreover, the baseline data used for computing fair RPSS, along with the other four strategies (namely S5, B-S5, B-E5 and P), was ECMWF ERA5 climatology. In addition, in the cases where the tercile category cannot be determined (e.g., both tercile thresholds are zeros), we assign zeros because only the highest positive fair RPSS is interesting in the final comparison. Regarding the P prediction, it is worth noting that we assigned one (100 %) to the tercile category in which the prediction belonged due to the lack of ensemble members. As such, the annual fair RPSS would be either one (perfect prediction) or negative values (prediction without added values).

Results and discussions

Given the characteristics of the five indicators, the following discussions are categorized into two groups: Section 4.1 for the SPR32, SU36 and SU40 indicators involving a threshold and the two indicators associated with an average condition (i.e., SPRTX and GST) in Section 4.2. The observed climatology of the indicators for the entire hindcast period was first presented and followed by the comparison of the ensemble-mean correlation coefficient and fair RPSS in each initialization date among the different strategies (except for the E5). The

differences between indicators, strategies and start months were assessed. The remaining bias of each indicator could be found in the supplementary material (see Fig. s1 & s2).

Threshold-defined indicators

These three indicators represent the locations of the potential heat stress in spring and summer, respectively. Even though the temperatures of crossing points depended on seasons (32 °C for spring; 36 °C and 40 °C for summer), the overall spatial patterns were similar: hotter in the southern half and cooler in the northwestern areas as shown in Fig. 3. In the Guadalquivir Valley, the SPR32 were above 12 days and the SU36 (SU40) could be more than 25 (5) days in summer. The second-highest hot spots were located in the region northwest to the Guadalquivir Valley and the Ebro Valley.

Fig. 4 shows the correlation coefficients of the S5, B-S5, B-E5 and P predictions of the SU36 and SU40 indicators. As expected, the steadily increasing correlation was seen when more observations were included in the calculation of the indicators along with the progressing season. As for SU36, S5 and B-E5 could have up to 0.5 of correlation at SM06 while P had a higher correlation over the southeastern areas. After that, when the season progressed to July (with the 21st – 30th of June included), B-E5 was improved particularly over the southeastern and south-central areas. At the same time, B-S5 showed an enhancement to a lesser extent basically in the southeastern region while P had fewer improvements only in the northeastern parts. Furthermore, there were much higher correlations for all three cases (i.e., B-S5, B-E5 and P) over a widespread region at SM08 when July was further combined. This marked increase in correlation indicates that July could be a decisive month for the SU36 indicator (and SU40 too). Although the three predictions attained a correlation above 0.7 almost across the entire domain, B-E5 performed slightly better than the other two.

The variabilities of correlation of the SU40 indicator were similar to SU36. However, partially due to its more extreme threshold, B-S5 did not have a comparable level of correlation to B-E5 throughout the months. At SM07, the correlation of B-E5 could reach around 0.6 in the Guadalquivir Valley and its northwestern region while B-S5 had a poorer performance (even when compared with P). Moreover, when above 0.8 of correlation could be seen in the southern peninsula for B-E5 and P at SM08, B-S5 showed limited values in a smaller area. Here, the fact that the improved performances of B-E5 and P due to the increasing share of observation relatively remained unchanged suggests that these two methods are less affected by the level of the extremeness of the used threshold. Conversely, B-S5 achieved a lower correlation in the latter months of the period for the SU40 indicator than SU36. This situation was also seen in the SPR32 indicator (see Fig. s3). May is critical for SPR32 (see Fig. s4).

A positive fair RPSS would encourage end-users to use the corresponding prediction in their decision-making because of the added value when compared to the use of climatology. Overall, the fair RPSS was steadily increased with the increasing proportion of observations for both indicators and all three strategies (B-S5, B-E5 and P) as shown in Fig. 5. As for SU36, B-S5 outperformed B-E5 and P in the first two months with a fair RPSS of up to 0.4 mainly over the southern region. However, B-E5 surpassed B-S5 at SM08 and SM09 when more observations were included, in particular the decisive July. Nevertheless, the fair RPSS of B-S5 at SM08 and SM09 kept increasing to 0.6–0.8 in the southern half (particularly in the Guadalquivir Valley and the Ebro Valley). Regarding P's performance, the fair RPSS of above 0.6 was widespread in a large area at SM09 while being relatively scattered at SM08.

Less predictability in the SU40 indicator was seen in the first two months for all the strategies probably due to the stricter threshold, and there were fewer days before summer in which the temperature maximum could exceed the threshold. As such, there were barely positive skills throughout the domain, but it is noteworthy that, in this case,

Climatology | ERA5 | 1993–2016

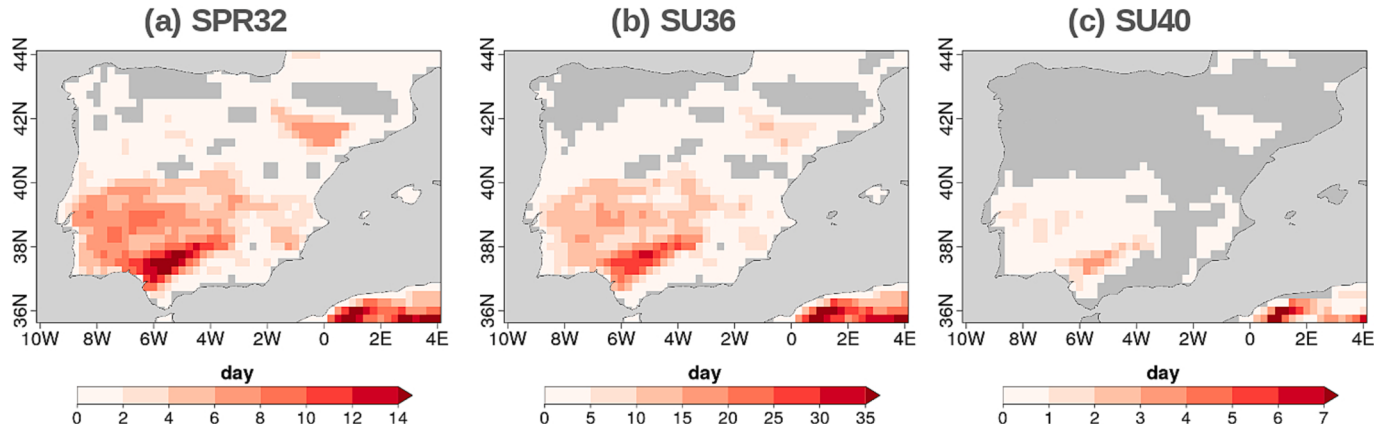


Fig. 3. ERA5 climatology for the threshold-defined indicators over the Iberian Peninsula from 1993 to 2016: (a) SPR32 (total number of days with daily maximum temperature above 32 °C from 21st April to 21st June), (b) SU36 and (c) SU40 (total number of days with the daily maximum temperature above 36 °C/40 °C from 21st June to 21st September). Darker grey shadings indicate the grid points where the temperatures were consistently below the thresholds in the observation.

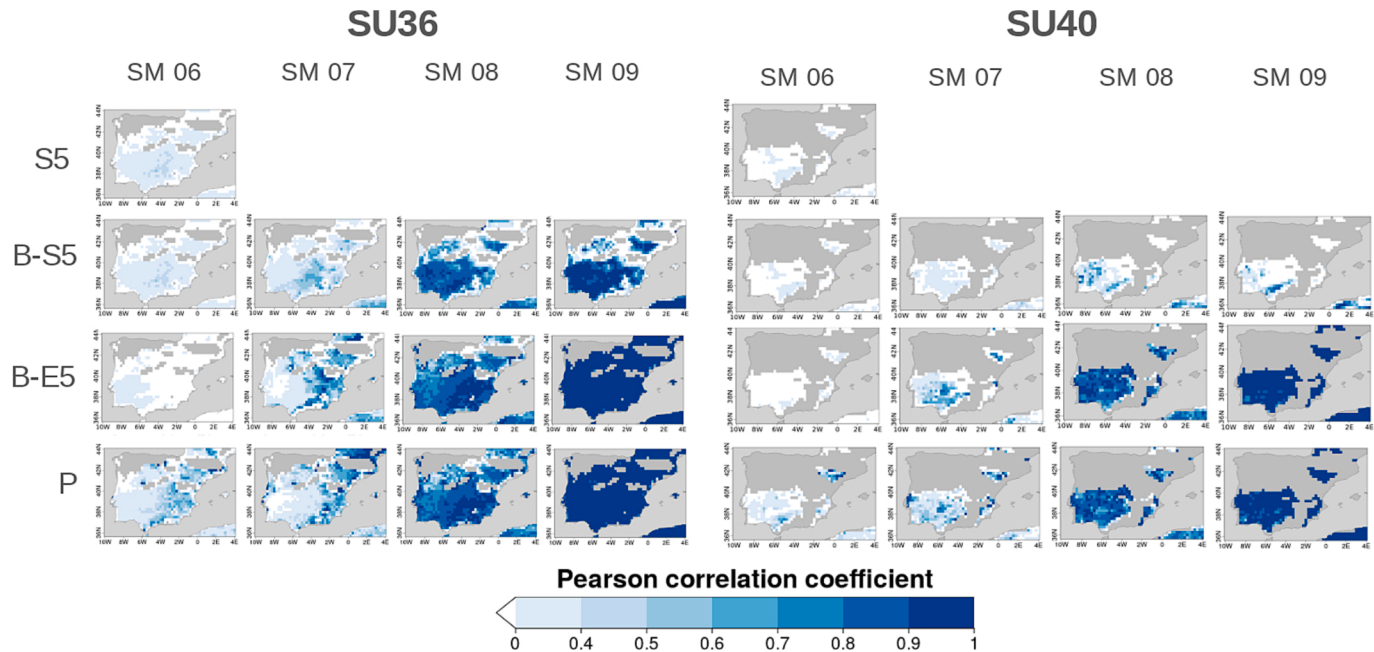


Fig. 4. Pearson's correlation coefficients (r) of the S5, B-S5, B-E5 and P predictions of the (left) SU36 and (right) SU40 indicators for the start months from June (SM06) to September (SM09). Darker grey shadings indicate the grid points where the temperatures were consistently below the thresholds in the observation. Only positive correlation coefficients are shown in blue. (For interpretation of the references to color in this figure legend, the reader is referred to the web version of this article.)

future use of ‘in-field observations’ could provide a way to ameliorate the results of the blending strategy (especially in terms of operative application). When the season went into August, B-S5 had the best fair RPSS of above 0.4 in the southwestern region and the Ebro Valley and continued to increase in September. At last, P showed positive fair RPSS over the Guadalquivir Valley and its northwest in the last two months. The months and locations being in favor of using seasonal forecasts depend on the indicator and location. For example, SU36 over the southern IP and the Ebro Valley at SM07 and SM08 and SPR32 over the southwest of IP at SM06 (see Fig. s4) could be highlighted according to fair RPSS. As such, according to Table 1, the need for irrigation from late spring to summer as well as the protection from extremely hot days could be improved or prepared in advance by using seasonal forecasts (B-S5).

Period-average indicators

The SPRTX and GST indicators represent the average temperature condition in spring (April–May) and from spring to autumn (April–October), respectively. Moreover, the former considers only the maximum temperature while the latter takes the mean of maximum and minimum temperatures. Fig. 6 manifests the observed climatology of the two indicators over IP for the 1993–2016 period. The spatial patterns were analogous to the maximums seen in the Guadalquivir Valley (above 24 °C for SPRTX and 22–24 °C for GST) and the minimums around the Pyrenees of below 12 °C.

As seen in the threshold-defined indicators, the correlation coefficients of the period-average indicators also show a consistent increase with more observations added in all the cases. Overall, the order

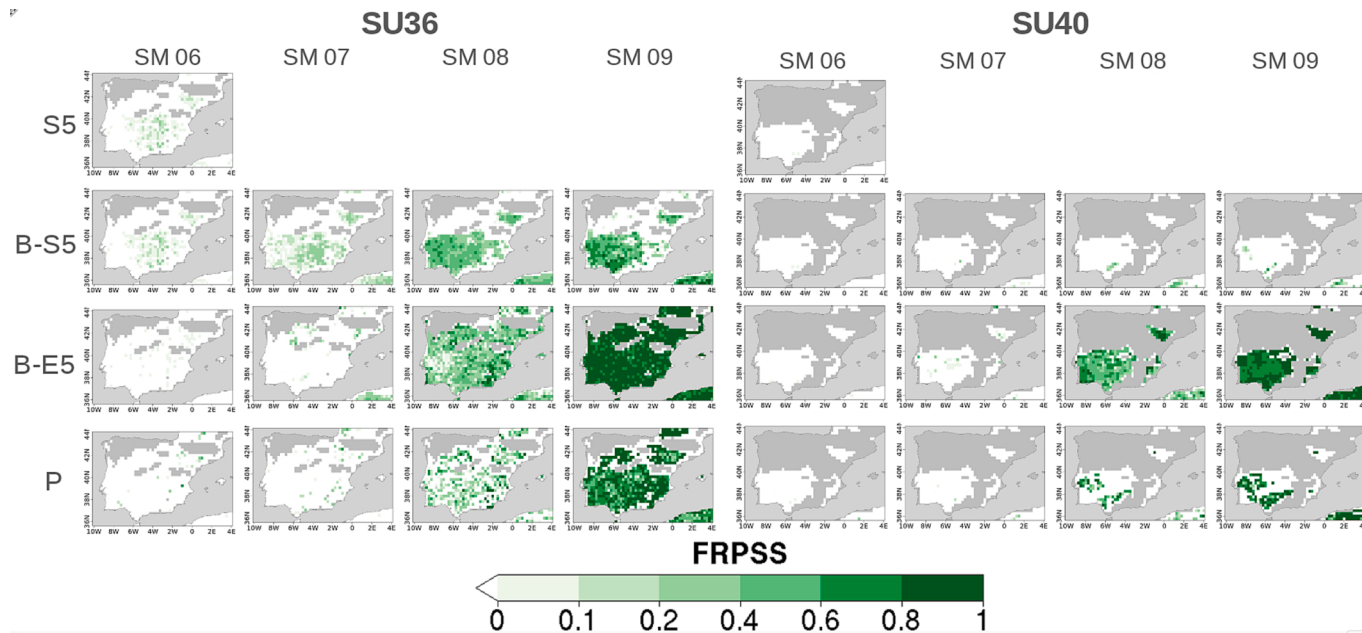


Fig. 5. Fair RPSS of SU36 and SU40 indicators of the four strategies: S5, B-S5, B-E5 and P from top to bottom. The start months range from June (SM06) to September (SM09) from left to right. Darker grey shadings indicate the grid points where the temperatures were consistently below the threshold in the observation. Only positive values are shown in green. (For interpretation of the references to color in this figure legend, the reader is referred to the web version of this article.)

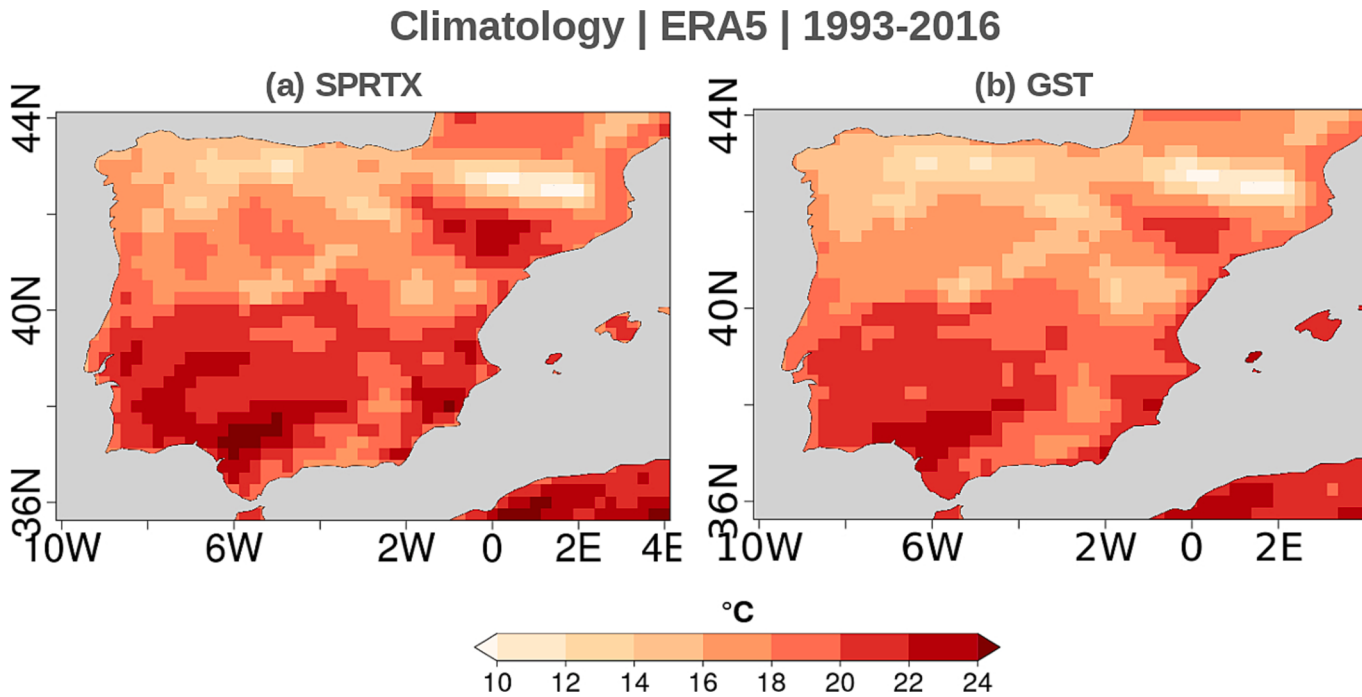


Fig. 6. ERA5 climatology of the (a) SPRTX (average maximum temperature from April to May) and (b) GST (7-month mean of the average of daily maximum and minimum temperatures from April to October) indicators over IP for the 1993–2016 period.

of the performance among the three strategies was basically B-S5 > P > B-E5. For B-S5, the correlations of GST were up to 0.5 in April (SM04) and were increased to above 0.9 throughout the entire domain at SM10 in Fig. 7. SPRTX attained correlations of above 0.7 in SM05 when April observation was included (see Fig. s5).

The high fair RPSS of the B-S5 shown in Fig. 8 confirms the out-performance of B-S5. This is also seen in SPRTX in Fig. s6. More importantly, B-S5 was predominant in April and kept outperforming over a broad region throughout the seven months. Actually, the

difference between B-S5 and B-E5 seemed to decrease between SM07 and SM10. Besides, May could be the decisive month to obtain the forecasting skill for B-E5 while P attained positive fair RPSSs after the first three months were included. This could hint that a longer observation is required for P to surpass climatology (see the bottom row). SPRTX basically has the same finding as GST (see Fig. s6).

It is worth noting that using seasonal forecasts with the blending approach is more likely to outperform the other strategies in the earlier months of the defined period. However, this superiority was found to

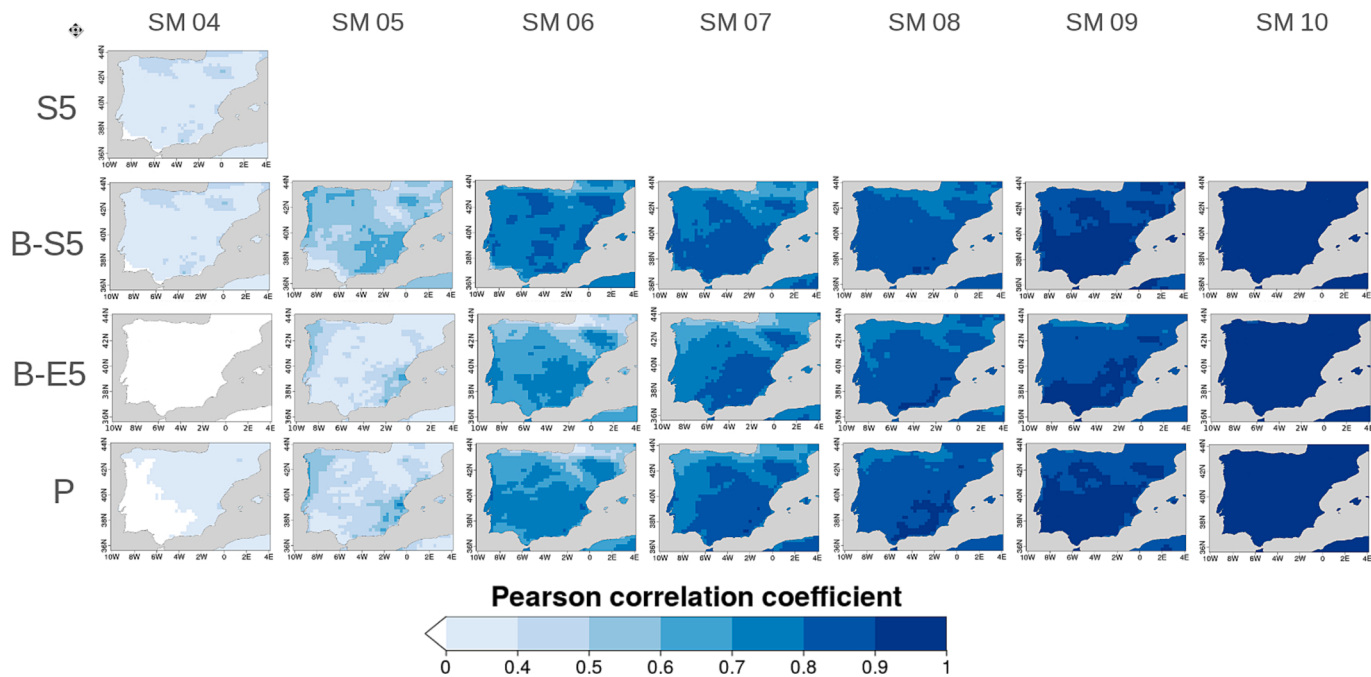


Fig. 7. Pearson's correlation coefficients (r) of the S5, B-S5, B-E5 and P predictions (top to bottom) of the GST indicator from the start months April (SM04) to October (SM10) (left to right). Only positive correlation coefficients are shown here.

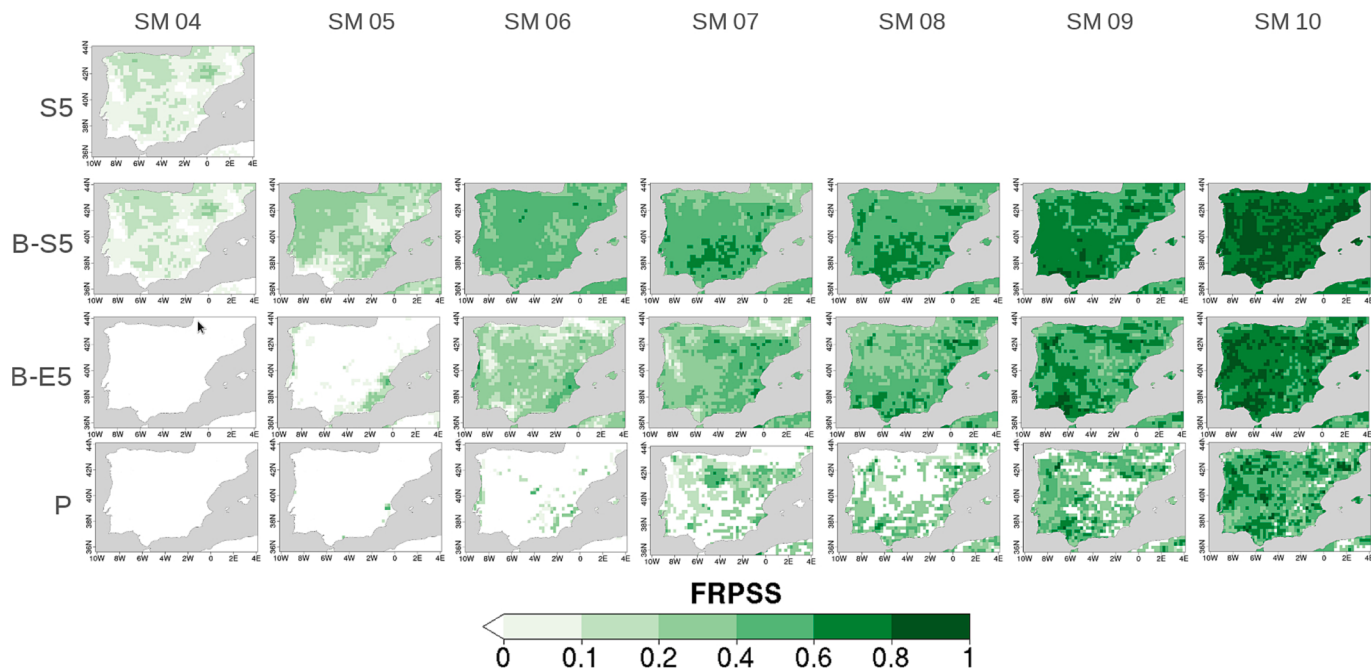


Fig. 8. Fair RPSS of the GST indicator of the four strategies: S5, B-S5, B-E5 and P (top to bottom). The start months range from April (SM04) to October (SM10) from left to right. Only positive fair RPSSs are shown here.

shrink with the increasing share of observations included in the computation of each indicator. This reduction in FRPSS could be foreseen because the baseline climatology and the predictions progressively became more similar as more observations were introduced and, hence, this decreased the room for improvement.

Conclusions

This study analyzed the potential usage of seasonal predictions in the olive sector in the Iberian Peninsula (IP) by applying five seasonal

prediction strategies to five sectoral bioclimatic indicators (SPR32, SU36, SU40, SPRTX, GST). In addition to the commonly used climatology and seasonal predictions, both of them were also combined with the actual observations once they became available (blending strategy). Besides, the persistence method was added in the comparison. After that, the behavior of the verification skill metrics was then analyzed for each initialization date as well as for each indicator and forecast strategy.

The results show that, for all the indicators, blending either seasonal predictions or climatology with observations enhanced the capability of

forecasting the tercile category when compared with the use of climatology or seasonal predictions alone. Furthermore, the decisive month to obtain a marked increase in the skill metric could be identified: May for SPR32; July for SU36 and SU40; and May for GST.

For the threshold-defined indicators, B-E5 tends to be more skilful over a wider area than the other methods. As seen in Fig. 4 and Fig. 5, the inclusion of the decisive month largely enhanced both verification metrics of the B-E5 than the other methods. Conversely, P could outperform climatology in the later start months. As for the period-average indicators (i.e., SPRTX and GST), the B-S5 was the best prediction in most start months although B-E5 could have a comparable skill.

To better visualize the spatial variabilities of the best strategy throughout the indicator target period, Fig. 9 and Fig. 10 illustrate the performer with the highest fair RPSS in each grid point for each indicator in each start month. Each strategy corresponds to one color: green for B-S5, light green for S5, blue for B-E5, light blue for E5 and yellow for P.

Overall, the best prediction for the threshold-defined indicators was changed from the E5 to B-E5 or a mixture of B-S5 and B-E5 with the increasing share of observations within the indicators. For example, E5

outperformed the other methods in the first month for all three indicators and also in the second month for SPR32 and SU40. The S5 and B-S5 for SU36 could have the highest fair RPSS over the southern areas in the SM06 and SM07, respectively, although E5 could be seen in the rest regions. When the season progresses, with more available observations, the B-E5 starts to appear. For instance, the B-E5 could be found in a widespread region for SU36 and SU40 in SM08 and SM09 while the B-S5 is predominant over the southwestern IP in SM08. Additionally, there is a mixture of B-E5, B-S5 and P for the last month of SPR32. The fact that B-S5 only exists for SPR32 and SU36 may indicate the difficulty for B-S5 to surpass B-E5 when the used threshold is too extreme (40 °C).

On the other hand, for the period-average indicators, as shown in Fig. 10, the S5 was predominant in the first month and B-S5 basically had the highest fair RPSS across the entire IP in the remaining months (except for SPRTX in SM05) in particular for GST. Even so, B-E5 could appear in scattered locations for GST from SM07 to SM10. Also, B-E5 could be found across the entire IP for SPRTX in SM05 while B-S5 has comparable fair RPSS as B-E5 (see Fig. s6). Unlike the threshold-defined indicators, the B-S5 strategy tends to have more skill in the period-average group. However, its superiority when compared to B-E5 also diminished in the latter months of the defined period (e.g., SPRTX in

Predominant prediction of each start month (the threshold-defined indicators)

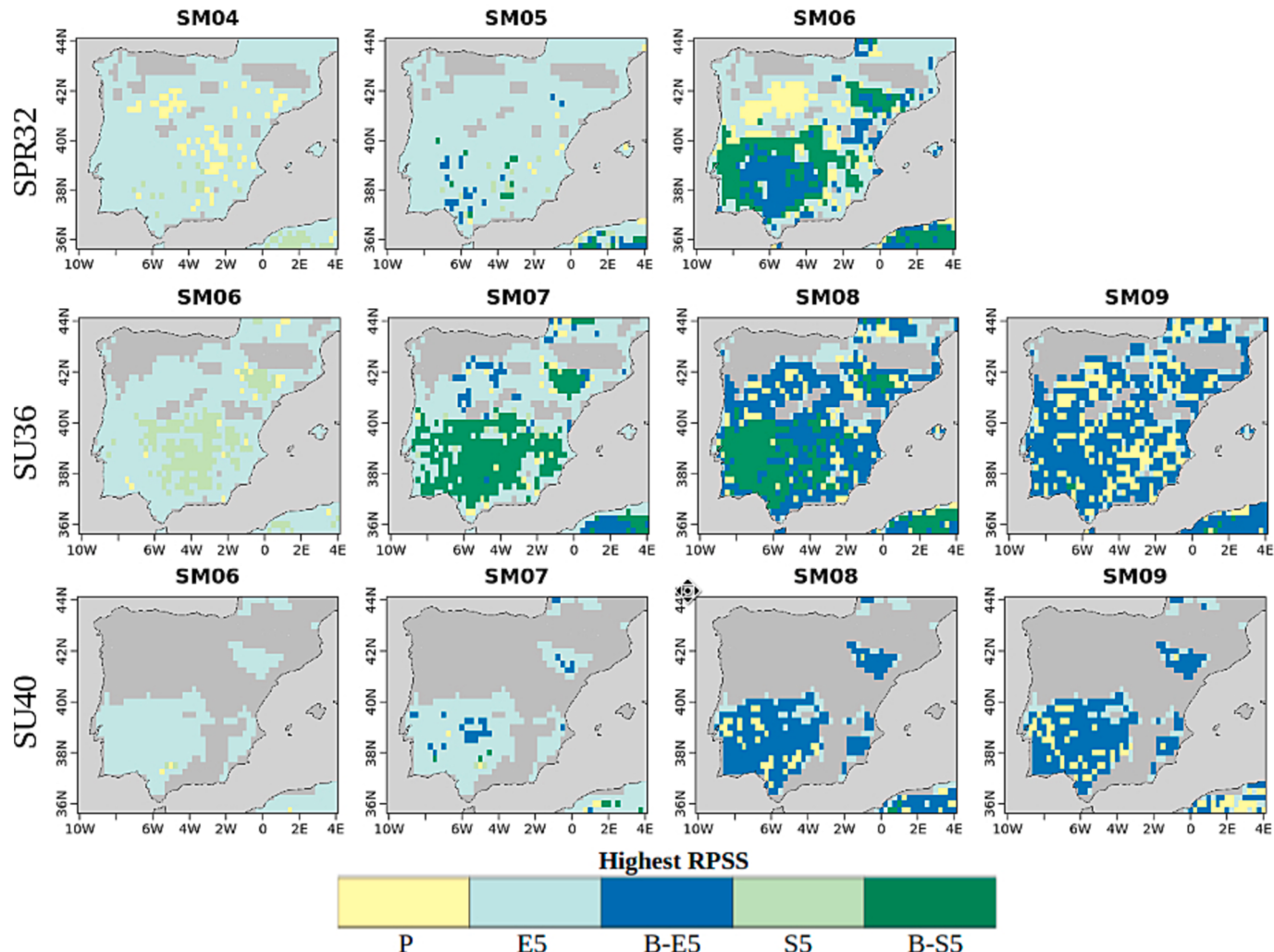


Fig. 9. The strategy with the highest fair RPSS in each start month (left to right) of the three threshold-defined indicators: SPR32, SU36 and SU40 (from top to bottom). The start months of SPR32 (SU36 and SU40) range from April to June (June to September). Each strategy corresponds to one color: green for B-S5, light green for S5, blue for B-E5, light blue for E5 and yellow for P. Darker gray shadings indicate the grid points where the observed temperatures are below the threshold throughout the defined period. (For interpretation of the references to color in this figure legend, the reader is referred to the web version of this article.)

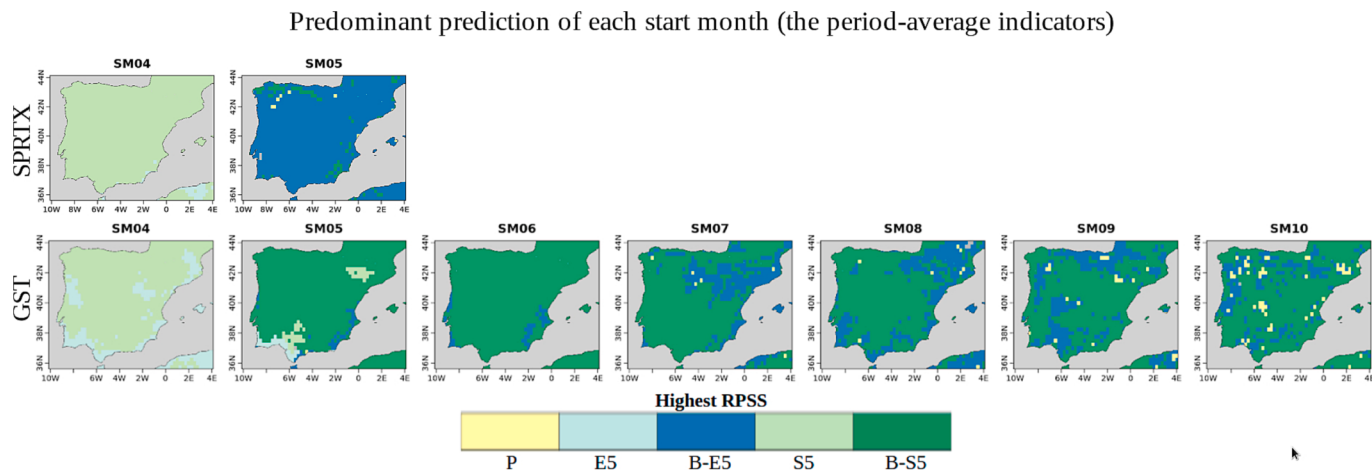


Fig. 10. Same as Fig. 9 but for the period-average indicators: SPRTX (from April to May) and GST (April–October).

Fig. s5 and s6; SM09 of SU36 and SM08 and SM09 of SU40 in Fig. 4). This finding is expected because the majority of the ‘blended’ prediction for both strategies corresponds to the same past observational data for these start dates. Therefore, this has to be considered when selecting the strategy for those indicators in the latter months.

To conclude, when seasonally predicting bioclimatic indicators for the olive sector, it is highly recommended to uptake the available observations as the indicator period progresses. On the one hand, the end-users are encouraged to combine the observations with SEAS5 predictions for the period-average indicators (GST and SPRTX). On the other hand, when it comes to an indicator defined by a fixed threshold (SPR32, SU36 and SU40), the observed climatology would be a suitable option for the first month and it should also be combined with observations as soon as they become available. Besides, the persistence-derived prediction could be considered only in the later month(s).

The above findings provide the olive sector end-users with a general guideline to make the most of the seasonal predictions of their sectoral bioclimatic indicators (by taking advantage of all the possible usage options of the information already available).

CRediT authorship contribution statement

Chihchung Chou: Data curation, Formal analysis, Visualization, Investigation, Writing – original draft. **Raúl Marcos-Matamoros:** Conceptualization, Investigation, Supervision, Writing – review & editing. **Javier López-Nevado:** Writing – review & editing. **Silvia López-Feria:** Writing – review & editing. **Nube González-Reviriego:** Conceptualization, Supervision.

Declaration of Competing Interest

The authors declare that they have no known competing financial interests or personal relationships that could have appeared to influence the work reported in this paper.

Data availability

Data will be made available on request.

Acknowledgements

Thanks to all the partners of the project MED-GOLD (Turning climate-related information into added value for traditional Mediterranean Grape, Olive and Durum Wheat food systems, agreement no. 776467) and the project ASPECT (HE-101081460) both funded by the European Union. Thanks to Dcoop as the end-user for providing

feedback in the co-development process. The results contain modified Copernicus Climate Change Service information. Neither the European Commission nor ECMWF is responsible for any use that may be made of the Copernicus information or data it contains. One of the coauthors, Raúl Marcos-Matamoros, is a Serra Húnter Fellow. Finally, we thank the reviewers, whose comments helped improve the paper substantially.

Appendix A. Supplementary data

Supplementary data to this article can be found online at <https://doi.org/10.1016/j.ciser.2023.100345>.

References

- Benloch-González, M., Sánchez-Lucas, R., Benloch, M., & Fernández-Escobar, R. (2019). Chapter III. Global warming effects on reproductive and vegetative phases of olive trees growing under field conditions. The effect of increasing temperature on olive trees (*Olea europaea* L. subsp. *europaea*) biology: An integrated morphological, phenological and biomolecular study, 29.
- Besnard, G., Khadari, B., Navascués, M., Fernández-Mazuecos, M., El Bakkali, A., Arriaga, N., Baali-Cherif, D., Brunini-Bronzini de Caraffa, V., Santoni, S., Vargas, P., Savolainen, V., 2013. The complex history of the olive tree: from Late Quaternary diversification of Mediterranean lineages to primary domestication in the northern Levant. Proc. R. Soc. B Biol. Sci. 280 (1756), 20122833.
- Besnard, G., Terra, J.F., Cornille, A., 2018. On the origins and domestication of the olive: a review and perspectives. Ann. Bot. 121 (3), 385–403. <https://doi.org/10.1093/aob/mcy002>.
- Brogli, R., Kröner, N., Sørland, S.L., Lüthi, D., Schär, C., 2019. The role of hadley circulation and lapse-rate changes for the future European summer climate. J. Clim. 32 (2), 385–404. <https://doi.org/10.1175/JCLI-D-18-0431.1>.
- Carvalho, D., Cardoso Pereira, S., Rocha, A., 2021. Future surface temperatures over Europe according to CMIP6 climate projections: an analysis with original and bias-corrected data. Clim. Change 167 (1), 1–17. <https://doi.org/10.1007/s10584-021-03159-0>.
- Casanueva, A., Bedia, J., Herrera, S., Fernández, J., Gutiérrez, J.M., 2018. Direct and component-wise bias correction of multi-variate climate indices: the percentile adjustment function diagnostic tool. Clim. Change 147 (3), 411–425. <https://doi.org/10.1007/s10584-018-2167-5>.
- Ceglar, A., Toreti, A., 2021. Seasonal climate forecast can inform the European agricultural sector well in advance of harvesting. npj Climate and Atmospheric Science 4 (1), 1–8. <https://doi.org/10.1038/s41612-021-00198-3>.
- Cook, B. I., Mankin, J. S., Marvel, K., Williams, A. P., Smerdon, J. E., & Anchukaitis, K. J. (2020). Twenty-first century drought projections in the CMIP6 forcing scenarios. Earth's Future, 8(6), e2019EF001461. doi: 10.1029/2019EF001461.
- Cos, J., Doblas-Reyes, F., Jury, M., Marcos, R., Bretonnière, P.A., Samsó, M., 2022. The Mediterranean climate change hotspot in the CMIP5 and CMIP6 projections. Earth Syst. Dyn. 13 (1), 321–340. <https://doi.org/10.5194/esd-13-321-2022>.
- Doblas-Reyes, F.J., Hagedorn, R., Palmer, T.N., 2005. The rationale behind the success of multi-model ensembles in seasonal forecasting—II. Calibration and combination. Tellus A: Dynamic Meteorol. Oceanogr. 57 (3), 234–252. <https://doi.org/10.3402/tellusa.v57i3.14658>.
- Ferro, C.A.T., 2014. Fair scores for ensemble forecasts. Q. J. R. Meteorol. Soc. 140 (683), 1917–1923. <https://doi.org/10.1002/qj.2270>.
- Fricker, T.E., Ferro, C.A., Stephenson, D.B., 2013. Three recommendations for evaluating climate predictions. Meteorol. Appl. 20 (2), 246–255. <https://doi.org/10.1002/met.1409>.

- Giannakopoulos, C., Gratsea, M., López-Neado, J., López-Feria, S., Sanderson, M. G., ZamoraRojas, R., Terrado M., Marcos R., Bruno Soares, M., Mihailescu, E., Arjona, R., Ponti, L., Calmanti S. (2019): MED-GOLD Deliverable 2.6 First feedback report from users on olive oil pilot service development. https://www.med-gold.eu/wp-content/uploads/docs/776467_MED-GOLD_DEL2.6_%20First-feedback-report-from-users-on-olive-oil-pilot-service.pdf.
- Giannakopoulos, C., Gratsea, M., López-Neado, J., López-Feria, S., López-Nevado, J., Ponti, L., Bruno Soares, M., Arjona, R., 2020. Second Feedback report from users on olive oil pilot service development. Zenodo. <https://doi.org/10.5281/zenodo.4543320>.
- Giorgi, F., Lionello, P., 2008. Climate change projections for the Mediterranean region. *Global Planet. Change* 63 (2), 90–104. <https://doi.org/10.1016/j.gloplacha.2007.09.005>.
- Gubler, S., Sedlmeier, K., Bhend, J., Avalos, G., Coelho, C.A.S., Escajadillo, Y., Jacques-Coper, M., Martinez, R., Schwierz, C., de Skansi, M., Spirig, C.H., 2019. Assessment of ECMWF SEAS5 seasonal forecast performance over South America. *Weather Forecast*. 35 (2), 561–584.
- Guioit, J., Cramer, W., 2016. Climate change: The 2015 Paris Agreement thresholds and Mediterranean basin ecosystems. *Science* 354 (6311), 465–468.
- Hayashi, K., Llorca, L., Rustini, S., Setyanto, P., Zaini, Z., 2018. Reducing vulnerability of rainfed agriculture through seasonal climate predictions: A case study on the rainfed rice production in Southeast Asia. *Agr. Syst.* 162, 66–76. <https://doi.org/10.1016/j.agryea.2018.01.007>.
- Hersbach, H., Bell, B., Berrisford, P., Hirahara, S., Horányi, A., Muñoz-Sabater, J., Nicolas, J., Peubey, C., Radu, R., Schepers, D., Simmons, A., Soci, C., Abdalla, S., Abellán, X., Balsamo, G., Bechtold, P., Biavati, G., Bidlot, J., Bonavita, M., Chiara, G., Dahlgren, P., Dee, D., Diamantakis, M., Dragani, R., Flemming, J., Forbes, R., Fuentes, M., Geer, A., Haimberger, L., Healy, S., Hogan, R.J., Hólm, E., Janisková, M., Keeley, S., Laloyaux, P., Lopez, P., Lupu, C., Radnoti, G., Rosnay, P., Rozum, I., Vamborg, F., Villaume, S., Thépaut, J.-N., 2020. The ERA5 global reanalysis. *Q. J. R. Meteorol. Soc.* 146 (730), 1999–2049.
- Hersbach, H., Bell, B., Berrisford, P., Biavati, G., Horányi, A., Muñoz-Sabater, J., Nicolas, J., Peubey, C., Radu, R., Rozum, I., Schepers, D., Simmons, A., Soci, C., Dee, D., Thépaut, J.-N. (2018). ERA5 hourly data on pressure levels from 1979 to present. Copernicus Climate Change Service (C3S) Climate Data Store (CDS). (Accessed on < 17-02-2020 >), 10.24381/cds.bd0915c6.
- Iizumi, T., Takaya, Y., Kim, W., Nakaegawa, T., Maeda, S., 2021. Global within-season yield anomaly prediction for major crops derived using seasonal forecasts of large-scale climate indices and regional temperature and precipitation. *Weather Forecast*. 36 (1), 285–299. <https://doi.org/10.1175/WAF-D-20-0097.1>.
- International Olive Council (2018) World Olive Oil Figures. <https://www.internationaloliveoil.org/what-we-do/economic-affairs-promotion-unit/#figures>. Assessed date: 29 Dec 2021.
- Iovane, M., Cirillo, A., Izzo, L.G., Di Vaio, C., Aronne, G., 2021. High temperature and humidity affect pollen viability and longevity in Olea europaea L. *Agronomy* 12 (1), 1. <https://doi.org/10.3390/agronomy12010001>.
- Johnson, S.J., Stockdale, T.N., Ferranti, L., Balmaseda, M.A., Molteni, F., Magnusson, L., Tietsche, S., Decremer, D., Weisheimer, A., Balsamo, G., Keeley, S.P.E., Mogensen, K., Zuo, H., Monge-Sanz, B.M., 2019. SEAS5: The new ECMWF seasonal forecast system. *Geosci. Model Dev.* 12 (3), 1087–1117.
- Kröner, N., Kotlarski, S., Fischer, E., Lüthi, D., Zubler, E., Schär, C., 2017. Separating climate change signals into thermodynamic, lapse-rate and circulation effects: theory and application to the European summer climate. *Clim. Dyn.* 48 (9), 3425–3440. <https://doi.org/10.1007/s00382-016-3276-3>.
- Kuglitsch, F.G., Toreti, A., Xoplaki, E., Della-Marta, P.M., Zerefos, C.S., Türkeş, M., Luterbacher, J., 2010. Heat wave changes in the eastern Mediterranean since 1960. *Geophys. Res. Lett.* 37 (4) <https://doi.org/10.1029/2009GL041841>.
- Lee, J.-Y., J. Marotzke, G. Bala, L. Cao, S. Corti, J.P. Dunne, F. Engelbrecht, E. Fischer, J. C. Fyfe, C. Jones, A. Maycock, J. Mutemi, O. Ndiaye, S. Panickal, and T. Zhou: 2021, Future Global Climate: Scenario-Based Projections and Near-Term Information. In Climate Change 2021: The Physical Science Basis. Contribution of Working Group I to the Sixth Assessment Report of the Intergovernmental Panel on Climate Change [Masson-Delmotte, V., P. Zhai, A. Pirani, S.L. Connors, C. Péan, S. Berger, N. Caud, Y. Chen, L. Goldfarb, M.I. Gomis, M. Huang, K. Leitzell, E. Lonnoy, J.B.R. Matthews, T. K. Maycock, T. Waterfield, O. Yelekçi, R. Yu, and B. Zhou (eds.)]. Cambridge University Press. In Press.
- Manzanas, R., Gutiérrez, J.M., Bhend, J., Hemri, S., Doblas-Reyes, F.J., Torralba, V., Penabad, E., Brookshaw, A., 2019. Bias adjustment and ensemble recalibration methods for seasonal forecasting: a comprehensive intercomparison using the C3S dataset. *Clim. Dyn.* 53 (3-4), 1287–1305.
- Marcos-Matamoros, R., González-Reviriego, N., Graça, A., Dell'Aquila, A., Vigo, I., Silva, S., Sanderson, M., 2020. Second Feedback report from users on wine pilot service development. Zenodo. <https://doi.org/10.5281/zenodo.5710836>.
- MED-GOLD, 2021: Infosheet CLIMATE SERVICES FOR THE OLIVE AND OLIVE OIL SECTOR, https://www.med-gold.eu/wp-content/uploads/docs/MED-GOLD_infosheet02_olivesoliveoil-EN.pdf.
- Molina, M.O., Sánchez, E., Gutiérrez, C., 2020. Future heat waves over the Mediterranean from an Euro-CORDEX regional climate model ensemble. *Sci. Rep.* 10 (1), 1–10. <https://doi.org/10.1038/s41598-020-65663-0>.
- Orlandi, F., Rojo, J., Picornell, A., Oteros, J., Pérez-Badia, R., Fornaciari, M., 2020. Impact of climate change on olive crop production in Italy. *Atmos.* 11 (6), 595. <https://doi.org/10.3390/atmos11060595>.
- Özdemir, Y., 2016. Effects of climate change on olive cultivation and table olive and olive oil quality. *Horticulture* 60, 65–69.
- Pérez-Zanón, N., C. Chihchung, and L. Lledó, 2021: CSIndicators: Sectoral Indicators for Climate Services Based on Sub-Seasonal to Decadal Climate Predictions, CRAN [online] Available from: <https://cran.r-project.org/package=CSIndicators>.
- Ranasinghe, R., A.C. Ruane, R. Vautard, N. Arnell, E. Coppola, F.A. Cruz, S. Dessai, A.S. Islam, M. Rahimi, D. Ruiz Carrascal, J. Sillmann, M.B. Sylla, C. Tebaldi, W. Wang, and R. Zaaboul, 2021: Climate Change Information for Regional Impact and for Risk Assessment. In Climate Change 2021: The Physical Science Basis. Contribution of Working Group I to the Sixth Assessment Report of the Intergovernmental Panel on Climate Change [MassonDelmotte, V., P. Zhai, A. Pirani, S.L. Connors, C. Péan, S. Berger, N. Caud, Y. Chen, L. Goldfarb, M.I. Gomis, M. Huang, K. Leitzell, E. Lonnoy, J.B.R. Matthews, T.K. Maycock, T. Waterfield, O. Yelekçi, R. Yu, and B. Zhou (eds.)]. Cambridge University Press. In Press.
- Raoult, B., Bergeron, C., Alós, A.L., Thépaut, J.N., Dee, D., 2017. Climate service develops user-friendly data store. ECMWF newsletter 151, 22–27. <https://doi.org/10.21957/p3c285>.
- Rodríguez Sousa, A.A., Barandica, J.M., Aguilera, P.A., Rescia, A.J., 2020. Examining potential environmental consequences of climate change and other driving forces on the sustainability of spanish olive groves under a socio-ecological approach. *Agriculture* 10 (11), 509. <https://doi.org/10.3390/agriculture10110509>.
- Sanderson, M. G., Giannakopoulos, C., Zamora-Rojas, E., Terrado, M., Gonzalez-Reviriego, N., Marcos, R., Bruno Soares, M., Arjona, R., Dell'Aquila, A., Ponti, L., Calmanti, S., Pasqui, M., Maglavera, S., 2019: MED-GOLD Deliverable 2.1 Report on the Knowledge capitalization of the olive oil sector. https://www.med-gold.eu/wp-content/uploads/docs/776467_MED-GOLD_DEL2.1_%20Knowledge-capitalization-Olive-Sector.pdf.
- Tognetti, R., d'Andria, R., Morelli, G., Calandrelli, D., Fragnito, F., 2004. Irrigation effects on daily and seasonal variations of trunk sap flow and leaf water relations in olive trees. *Plant and Soil* 263 (1), 249–264. <https://doi.org/10.1023/B:PLSO.0000047738.96931.91>.
- Von Storch, H., Zwiers, F.W., 2002. *Statistical Analysis in Climate Research*. Cambridge University Press.
- Weisheimer, A., Befort, D. J., MacLeod, D., Palmer, T., O'Reilly, C., & Strømmen, K. (2020). Seasonal forecasts of the twentieth century. *Bulletin of the American Meteorological Society*, 101(8), E1413–E1426. doi: 10.1175/BAMS-D-19-0019.1.
- Zimmermann, J., Hauck, M., Dulamsuren, C., Leuschner, C., 2015. Climate warming-related growth decline affects *Fagus sylvatica*, but not other broad-leaved tree species in Central European mixed forests. *Ecosystems* 18 (4), 560–572. <https://doi.org/10.1007/s10021-015-9849-x>.
- Zittis, G., Bruggeman, A., Lelieveld, J., 2021. Revisiting future extreme precipitation trends in the Mediterranean. *Weather Clim. Extremes* 34, 100380. <https://doi.org/10.1016/j.wace.2021.100380>.